University of Cologne

Institute of Physics II

Bachelor thesis

Challenging the existence of a vibron quasi-bound state in $CeCuAl_3$

Author:
Paul Rosenberger

Supervisors:
Prof. Dr. Paul H. M. van Loosdrecht
Prof. Dr. Mohsen Abd-Elmeguid
Dr. Andrea Severing

January 2015

Contents

Introduction

In this thesis, the crystal-field ground state wave functions of the non-centrosymmetric tetragonal rare earth compounds $CeAuAl_3$ and $CeCuAl_3$ are studied by soft X-ray absorption spectroscopy in the total electron yield mode.

Chapter 1 gives a short overview of the properties of rare earth compounds and the two systems under investigation.

In chapter 2, the crystal field is introduced. Its effects and especially the case of cerium in tetragonal point symmetry are presented.

The experimental technique used for the investigations in this thesis, soft X-ray absorption spectroscopy, the general experimental setup, as well as the question how the crystal-field ground state symmetry can be determined by this technique are the topics of chapter 3.

The results of the studies performed in the framework of this thesis are presented in chapter 4 and finally in chapter 5 a conclusion and an outlook are given.

1. Cerium 113 compounds

Cerium is a rare earth (4f) element with one electron in the 4f shell ($4f^1$). The properties of rare earth compounds are mainly determined by the 4f electrons. Some of them containing cerium or ytterbium are so called heavy fermion compounds. They exhibit interesting effects like the Kondo effect and unconventional superconductivity [1].
The compounds studied in this thesis are $CeAuAl_3$ and $CeCuAl_3$. Both are crystallizing in the non-centrosymmetric $BaNiSn_3$-type crystal structure (space group I4mm) [2]. The crystal structure is shown in fig. 1.1. These compounds attracted attention because of the observation of superconductivity in $CePt_3Si$ [3], a material which also crystallizes in a non-centrosymmetric structure.

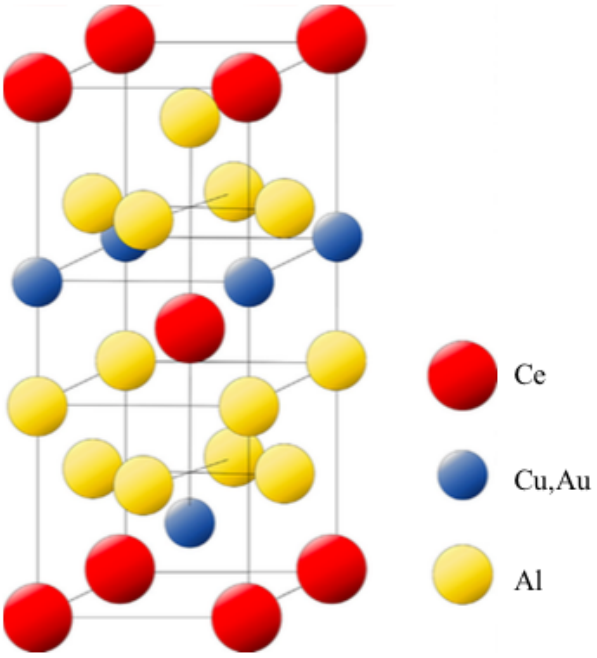

fig. 1.1. Crystal structure of Ce(Au, Cu)Al_3. Picture from [2]

$CeAuAl_3$ orders antiferromagnetically at $T_N = 1.32$ K. It exhibits a Kondo effect with a Kondo temperature of $T_K = 4.5$ K [4].

$CeCuAl_3$ has a Néel temperature of $T_N = 2.8$ K and a Kondo temperature of $T_K = 8$ K [5].

An increased interest in $CeCuAl_3$ is generated due to a publication by Adroja et al. [6]. By inelastic neutron scattering they found three excitations at 1.3 meV, 9.8 meV and 20.5 meV. Three excitations can not be described by the crystal field model since it only allows two excitations for cerium in tetragonal point symmetry (see section 2.2). They report that they were able to fit their features at 1.3 and 20.5 meV by the pure crystal-field model, but not the one at 9.8 meV and deduce that the existence of this state is due to electron-phonon coupling (vibron quasi-bound state) of a crystal-field excitation and a phonon mode. Thalmeier and Fulde developed a crystal-field-phonon coupling model to explain the presence of such a state in the cubic compound $CeAl_2$ [7]. Adroja et al. generalized this model to apply it to the present compound with tetragonal point symmetry. In this way, they succeeded in fitting all their spectral features.

The aim of this thesis is to study the crystal-field ground state of $CeAuAl_3$ and $CeCuAl_3$ as well as the presence of a vibron quasi-bound state in $CeCuAl_3$ by analyzing soft X-ray absorption data.

2. Crystal field

In this chapter an introduction to the crystal-electric field (CEF) and its influence will be given. The CEF is the electric field which is caused inside a solid by the charges of the ions surrounding the central ion. This thesis deals with two compounds where the central ion under investigation is a cerium ion. The ions are regarded as point charges in this model. This simple model was invented by H. Bethe [8] and J. H. van Vleck [9]. A more complex description is given by the Ligand field theory, where hopping of electrons between ligand atoms and the central ion can occur.
Cerium belongs to the rare earth series where the f shell is filled. As can be seen in fig. 2.1, the radii of the 4f orbitals are very small. Therefore hopping of these electrons can be neglected and the CEF theory is sufficient.

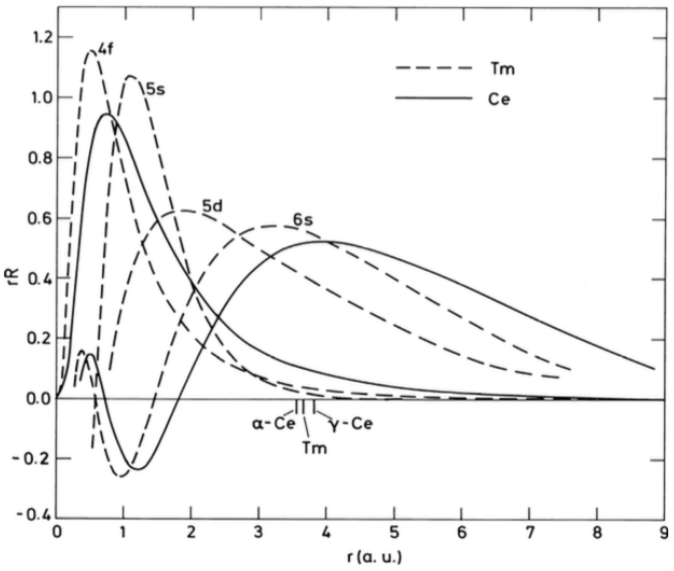

fig. 2.1. Radial distributions of the orbitals. From [10]

2.1. Effects of the crystal-electric field

In a free atom the electrons are only affected by the Coulomb potential of the core and the spin orbit interaction. If the ion is put into a solid, a CEF will also act on the ion, whereby the CEF depends on the symmetry of the crystal. The total Hamiltonian can be written as

$$H = H_{free} + V_{CEF} \tag{2.1}$$

The Hamiltonian of the free atom can be decomposed into its components and the magnitudes of the interactions can be compared to the magnitude of the CEF potential:

$$H = -\frac{\hbar^2}{2m}\sum_i \nabla_i^2 - \sum_i \frac{Ze^2}{r_i} + \frac{1}{2}\sum_{i\neq j}\frac{e^2}{r_{ij}} + \sum_i \zeta_i(r)\mathbf{l}_i\cdot\mathbf{s}_i + V_{CEF} \tag{2.2}$$

The last three summands are of interest since their hierarchy depends on the investigated elements. $\frac{e^2}{r_{ij}}$ is the Coulomb interaction and $\zeta_i(r)\mathbf{l}_i\cdot\mathbf{s}_i$ is the spin orbit interaction. For rare earths, the Coulomb interaction is strongest and the CEF potential is weakest:

$$V_{CEF} < \zeta_i(r)\mathbf{l}_i\cdot\mathbf{s}_i < \frac{e^2}{r_{ij}} \tag{2.3}$$

The differences are of the order of one magnitude (see fig. 2.2).
Coulomb repulsion causes multiplets. Since the eigenstates of the spin operator **S** and the operator of angular momentum **L** are eigenstates of the Coulomb operator, the multiplets can be described using the quantum numbers L and S.
The spin orbit coupling leads to a coupling of L and S resulting in the total angular momentum J ($J = L \mp S$). This LS-coupling scheme can be used, since the spin orbit coupling is small in comparison to the Coulomb repulsion. Thus, the multiplets are splitted into J-multiplets and L, S and J are good quantum numbers. The system can be described by Hund's rules. The Hund's rule states are (2J+1)-fold degenerate ($-J_z$ - $+J_z$) (see fig. 2.2) and have spherical symmetry.
The CEF lifts the degeneracy further and the total angular momentum J is no longer a good quantum number. Instead, the resulting eigenstates can be expressed as linear combination of J_z. These so called CEF states have no longer spherical symmetry (see

fig. 2.2).

2.2. Crystal-electric field of cerium in tetragonal symmetry

In this thesis cerium compounds are studied and thus the level splitting of cerium is discussed as an example. Cerium has one electron in the 4f shell ($4f^1$). Therefore the quantum numbers are as follows:

$$\begin{aligned} L &= 3 \\ S &= \frac{1}{2} \\ J &= L \pm S = \frac{7}{2}, \frac{5}{2} \end{aligned} \tag{2.4}$$

In total there are 14 possible states for the 4f electron. They are splitted into a $J = 7/2$ and a $J = 5/2$ multiplet by the spin orbit interaction. The $J = 5/2$ is the ground state, because the f-shell is less than half filled (3^{rd} Hund's rule). The $J = 7/2$ multiplet ist $(2 \cdot \frac{7}{2} + 1) = 8$-fold degenerate, the $J = 5/2$ one 6-fold. The degeneracy is reduced by the CEF. Fig. 2.2 shows the resulting level scheme. The CEF splits the $(2J + 1)$-fold degenerate states into 3 ($J = 5/2$) and 4 ($J = 7/2$) Kramer's doublets in case of tetragonal point symmetry.
The fourfold tetragonal axis, the c-axis, is the axis of highest symmetry and therefore it is useful to choose it as quantization axis. How does this symmetry now determine the eigenstates?
The eigenstates can be pure J_z states or mixtures of them. To mix two states, their quantum numbers $J_{z,1}$ and $J_{z,2}$ have to fulfil

$$\Delta J_z = |J_{z,1} - J_{z,2}| = n \tag{2.5}$$

where n is the order of the rotational symmetry axis, which is 4 for a tetragonal system. In this thesis full multiplet calculations are performed and the $J = 7/2$ multiplet is taken into account, but the intermixing of both multiplets is negligible because of the

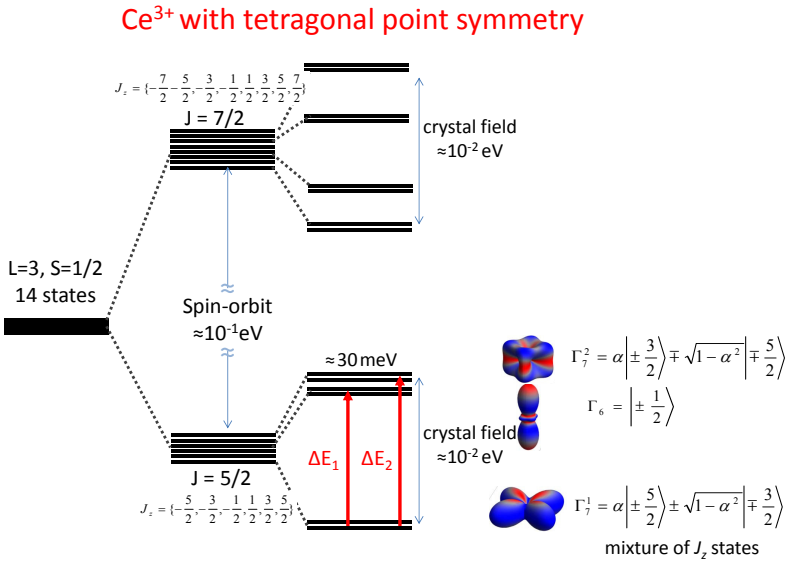

fig. 2.2. Level scheme of cerium with tetragonal point symmetry. The CEF splits the degenerate $J = 5/2$ and $J = 7/2$ multiplets into Kramer's doublets.

large spin orbit splitting of ≈ 280 meV. Hence, one only looks at how the CEF states can be expressed in a J_z-basis within the lowest $J = 5/2$ multiplet. The J_z quantum numbers are $-\frac{5}{2}$, $-\frac{3}{2}$, ..., $+\frac{5}{2}$.
According to eq. 2.5, the $\left|\pm\frac{1}{2}\right\rangle$ state can mix with a $\left|\mp\frac{7}{2}\right\rangle$ state, but for the reason described above, there is no $\left|\mp\frac{7}{2}\right\rangle$ state and thus the pure $\left|\pm\frac{1}{2}\right\rangle$ state is a CEF eigenstate. The $\left|+\frac{5}{2}\right\rangle$ state mixes with the $\left|-\frac{3}{2}\right\rangle$ state and the $\left|-\frac{5}{2}\right\rangle$ with the $\left|+\frac{3}{2}\right\rangle$. Therefore, the following states are CEF eigenstates and thus possible wave functions for cerium in tetragonal point symmetry:

$$\begin{aligned}
\Gamma_6 &= \left|\pm\frac{1}{2}\right\rangle \\
\Gamma_7^1 &= \alpha\left|\pm\frac{5}{2}\right\rangle \pm \beta\left|\mp\frac{3}{2}\right\rangle \\
\Gamma_7^2 &= \beta\left|\pm\frac{5}{2}\right\rangle \mp \alpha\left|\mp\frac{3}{2}\right\rangle
\end{aligned}$$

where $\alpha^2 + \beta^2 = 1$ and thus only the *mixing parameter* α has to be determined to describe the Γ_7 wave functions. In fig. 2.2 the angular distribution of these states is shown for $\alpha \approx 0.9$, demonstrating the strong anisotropy of the CEF wave function.

3. X-ray absorption spectroscopy

The experimental technique used for the studies in this thesis is soft X-ray absorption spectroscopy (XAS) in the total electron yield (TEY) mode. It is used to determine the CEF ground state.

3.1. Spectra and theory

In XAS measurements, a core shell electron is excited by a photon whose energy is in the range of the electron binding energy. Since these energies are element specific, XAS is an element specific technique. For rare earth compounds, whose properties are mainly determined by the 4f electrons, the transition from 3d to 4f (M-edge) yields the most interesting information about the ground state symmetry. The rare earth M-edges have binding energies from 800 to 900 eV, which is in the soft X-ray regime. Soft X-rays have a limited probing depth of about 40 Å so that sample surfaces have to be clean. This requires that samples are cleaved in situ and measurements are performed under ultra high vacuum of about 10^{-10} mbar. Cerium has one f electron (f^1) so that here the transitions from $|3d^{10}4f^1\rangle$ to $|3d^9 4f^2\rangle$ are studied.

3.1.1. Absorption spectra

First, a short description of an absorption spectrum will be given.
The XAS spectrum shows the transitions from the initial to the final states. For the intensity I, the following proportionality results from Fermi's golden rule:

$$I \propto \sum_{\psi_f} |\langle \psi_f | \hat{T} | \psi_i \rangle|^2 \delta(E_i + h\nu - E_f) \tag{3.1}$$

Here the absorption is described by the transition matrix

$$\langle\psi_f|\hat{T}|\psi_i\rangle \tag{3.2}$$

where ψ_i and ψ_f are the initial and the final state, respectively. $\hat{T}$ is the transition operator and can be expressed as

$$\hat{T} = e^{i\frac{\omega}{c}\hat{\mathbf{n}}\mathbf{r}}\mathbf{p}\cdot\hat{\mathbf{e}} \tag{3.3}$$

Here, $\hat{\mathbf{n}}$ is the light propagation vector, $\hat{\mathbf{e}}$ the light polarization vector, $\mathbf{r}$ the position of the excited electron and $\mathbf{p}$ its momentum.
$\hat{T}$ is expanded in a power series and only the first order term is taken into account. This is the so called dipole approximation and it is valid for soft X-rays because the spatial extension of the orbitals is large in comparison to the X-ray wavelength. The transition operator then simplifies to

$$\hat{T} \approx \mathbf{p}\cdot\hat{\mathbf{e}} = \hat{D} \tag{3.4}$$

and the intensity is

$$I \propto \sum_{\psi_f} |\langle\psi_f|\hat{D}|\psi_i\rangle|^2 \delta(E_i + h\nu - E_f) \tag{3.5}$$

The absorption spectra of cerium exhibits two absorption edges, M_4 and M_5, due to the 3d spin orbit splitting ($|3d^{10}4f^1\rangle \rightarrow \left|3d^9_{5/2}4f^2\right\rangle$ and $\left|3d^9_{3/2}4f^2\right\rangle$) (see top of fig. 3.1). The intensity of the M_5 edge is $\frac{3}{2}$ times as high as the M_4 edge, since the $J = \frac{5}{2}$ state is 6-fold degenerate, whereas the $J = \frac{3}{2}$ state is 4-fold degenerate.
There is only one initial state but many possible final states, giving rise to the underlying multiplet structure (see middle of fig. 3.1). Most of the final states are bound states as the interaction of the electron hole pair in the final state (exciton) is strong.
The peaks are broadened due to the experimental resolution and the final states' lifetime. The lifetime broadening is described by a Lorentzian, whereas the broadening due to the experimental resolution is described by a Gaussian (see bottom of fig. 3.1).
A few final states are non bound. They result in a continuum jump which can be

regarded as background.

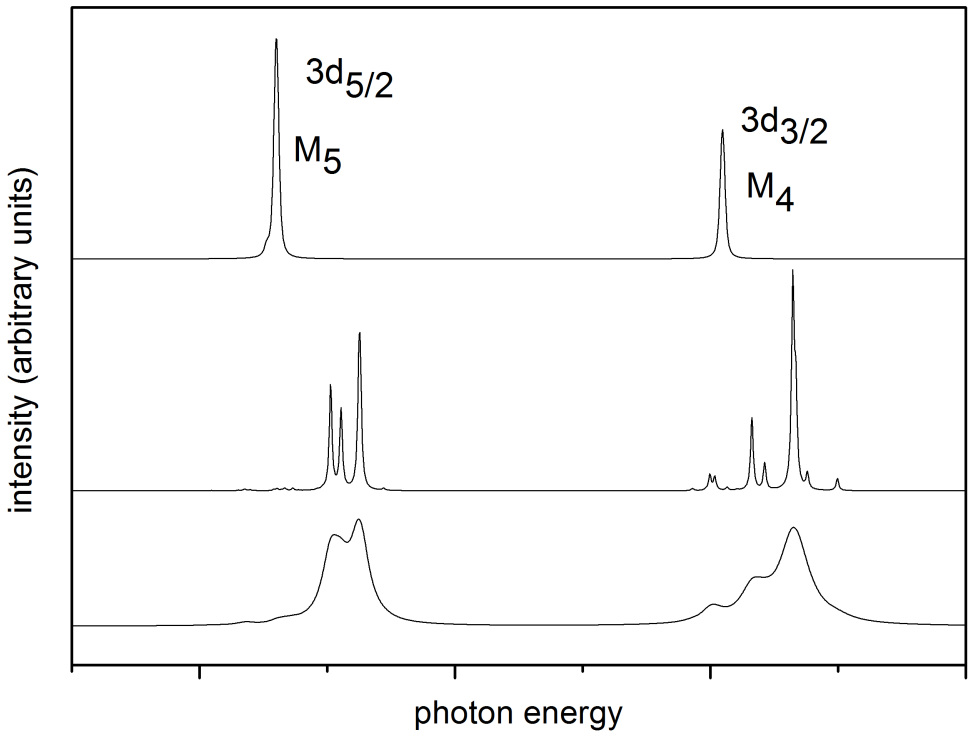

fig. 3.1. Simulated isotropic absorption spectra of $CeCuAl_3$ with electron-electron interactions (bottom) and without (top, scaled by a factor of 0.2). In the middle, the multiplet structure is shown (scaled by a factor of 0.3)

3.1.2. Dipole selection rules

The intensity is proportional to the square of $\langle\psi_f|\hat{D}|\psi_i\rangle$ which depicts an integral over the whole space so that the transition matrix $\langle\psi_f|\hat{D}|\psi_i\rangle$ has to be even. It would vanish in the case of an odd function. The wave functions of s (L=0) and d (L=2) orbitals are even, those of p (L=1) and f (L=3) orbitals are odd and the dipole operator $\hat{D}$ is also odd. Thus, 3d to 4f transitions are allowed and give high intensities in the XAS spectrum. There are further symmetry considerations leading to more selection rules:

$$\begin{aligned}\Delta l &= \pm 1\\ \Delta j &= 0, \pm 1\\ \Delta m_l &= 0, \pm 1\\ \Delta m_s &= 0\\ \Delta L &= 0, \pm 1\\ \Delta S &= 0\\ \Delta J &= 0, \pm 1\end{aligned}$$

In particular, the transition $d_{5/2} \rightarrow f_{5/2}$ fulfils $\Delta L{=}+1$ and $\Delta J{=}0$, and the transition $d_{3/2} \rightarrow f_{5/2}$ $\Delta L{=}+1$ and $\Delta J{=}+1$. Information about the initial state can be obtained from the absorption spectrum, since different initial states cause transitions into different final states.

3.1.3. Linear polarization and sensitivity to ground state symmetry

The dipole operator can be expressed as a linear combination of its components:

$$\hat{D} = \hat{D}_x + \hat{D}_y + \hat{D}_z \tag{3.6}$$

They describe the polarization directions of the light.
If only one component $\hat{D}_i$ is chosen, there is a kind of additional (symmetry) selection rule and thus additional information can be obtained.
The transition matrix $\langle\psi_f|\hat{D}_i|\psi_i\rangle$ depends on the shape of the initial and final state. In consequence, the linear dichroism (LD) - this is the difference between the absorption of light with polarization vectors parallel and perpendicular to a given axis - is sensitive to the ground state symmetry (ground state wave function). For rare earth compounds, this effect is strong and can be exploited to determine the CEF ground state symmetry [11]. Fig. 3.2 (left) shows simulations of the M-edges for the pure J_z states, $\left|\pm\frac{5}{2}\right\rangle$, $\left|\mp\frac{3}{2}\right\rangle$ and $\left|\pm\frac{1}{2}\right\rangle$. Each state has its own specific polarization.
In section 2.2 the possible CEF wave functions for cerium in tetragonal point symmetry have been introduced. The simulations in fig. 3.2 show that it is obviously possible to distinguish between a pure $\left|J_z = \pm\frac{1}{2}\right\rangle$ and a mixture of $\left|J_z = \mp\frac{3}{2}\right\rangle$ and $\left|J_z = \pm\frac{5}{2}\right\rangle$.

In the framework of this thesis, linear polarized spectra for $\mathbf{E}\|c$ and $\mathbf{E}\perp c$ have been measured. Here, $\mathbf{E}$ is the electric field vector which refers to the polarization direction of the light and c is the fourfold tetragonal axis. For modeling, the *isotropic spectrum* will also be used. It is constructed from the experimental linear polarized data as

$$I_{iso} = \frac{I_{\|c} + 2 \cdot I_{\perp c}}{3} \tag{3.7}$$

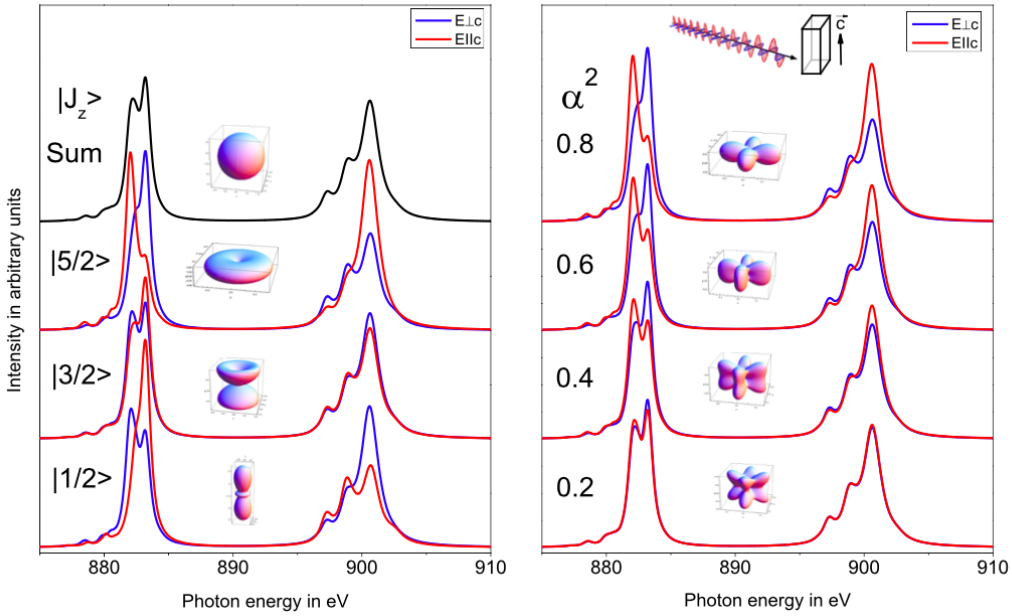

fig. 3.2. Polarization dependent XAS spectra of the pure J_z states (left) and mixed states (right). From [12].

3.1.4. Calculation of a X-ray absorption spectrum for a $4f^1$ system

Cluster calculations

The absorption spectra are simulated by cluster calculations. Since they are not ab initio, there are some parameters that have to be determined [13]. These are:

- spin orbit coupling of the
  - 4f electrons in the initial and in the final state. The associated spin orbit coupling constant is $\zeta_{4f}^{initial/final}$

  - 3d core hole in the final state with the spin orbit coupling constant ζ_{3d}^{final}

- Coulomb interaction between
  - the two 4f electrons in the final state. The interaction is described by the Slater integrals Rk_{4f}^{final}, where $k = 2, 4, 6$.
  - the 3d core hole and the 4f electron (exciton) with the associated Slater integrals Rk_{3d4f}^{final}, $k = 1, 2, 3, 4, 5$.

These atomic parameters can be obtained by Hartree-Fock calculations, using e.g the code by R. Cowan [14], but have to be adjusted for solids. The corrections are made by fitting the isotropic spectrum, which is nearly unaffected by the CEF effect (see [15]), because the CEF splitting in cerium compounds is of the order of 10 to 50 meV which is negligible compared to the lifetime broadening.
After reduction factors for the four parameters are determined, the CEF ground state symmetry can be studied by fitting the polarization dependent spectra.

Changes of spectra with temperature

The total absorption spectrum is the superposition of the spectra of the pure states. The possible wave functions for cerium in tetragonal point symmetry are mentioned in section 2.2. Assuming only the ground state to be populated and to be Γ_7^1, the spectral intensity, according to eq. 3.5 is [1]:

$$I = \alpha^2 I_{\pm\frac{5}{2}} + \beta^2 I_{\mp\frac{3}{2}} \tag{3.8}$$

$I_{\pm\frac{5}{2}}$ is the intensity of the pure $\left|J_z = \pm\frac{5}{2}\right\rangle$ state and $I_{\mp\frac{3}{2}}$ the intensity of the pure $\left|J_z = \mp\frac{3}{2}\right\rangle$ state.
The total intensity at higher temperatures follows Boltzmann statistics. Assuming n states, the occupation number N_j of the j^{th} state at a certain temperature T is thus defined as follows:

$$N_j(T) = \frac{e^{-\frac{E_j}{k_B T}}}{\sum_{i=0}^{n-1} e^{-\frac{E_i}{k_B T}}} \tag{3.9}$$

[1] Interference effects vanish for tetragonal point symmetry and CEF splittings small with respect to the spin-orbit splitting [15].

The total intensity at this temperature is then:

$$I_{tot} = \sum_{j=0}^{n-1} N_j I_j \tag{3.10}$$

From this is clear that the polarization dependent absorption spectra are changing with temperature due to the occupation of states. In the present case of cerium in tetragonal point symmetry, systems with 3 states are studied. Furthermore, to simulate the system with a vibron quasi-bound state, a fourth state has to be included (see section 4.3.2).

3.2. Experiment

XAS experiments are performed at synchrotrons since they deliver light that fulfils the requirements of this technique, which are:

- high brilliance
- tuneability
- stability
- reproducibility

3.2.1. Synchrotron radiation and experimental setup

Synchrotrons are particle accelerators. The particles are accelerated by electric fields and their paths are bend by magnetic fields. These fields are synchronized such that the particles are kept on a constant circular orbit while being accelerated. The particles have to be charged to be accelerated and charged particles on a circular orbit emit electromagnetic radiation. This radiation is called synchrotron radiation and was discovered in 1946 as an unwanted side effect. In the 70's its usefulness was recognized and the first electron synchrotrons were built in order to produce synchrotron radiation.

Modern synchrotrons consist of an electron gun, a linear accelerator, a booster ring and a storage ring as well as the beamlines with the experimental stations. The layout of such a synchrotron is shown in fig. 3.3. The linear accelerator accelerates the electrons from the electron gun and injects them into the booster ring where they are accelerated

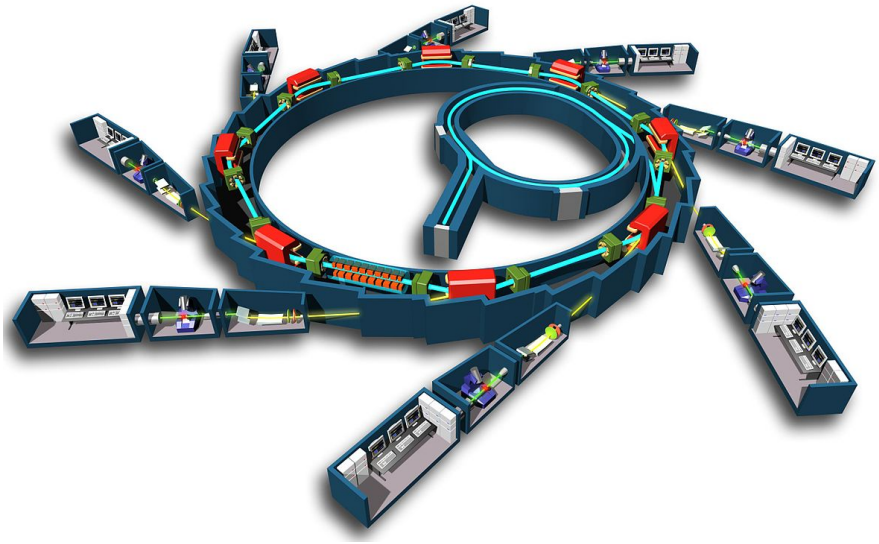

fig. 3.3. Schematic depiction of a synchrotron. From [16]

up to nearly the speed of light, before the electrons are injected into the storage ring. The synchrotron radiation is emitted at the bending magnets and can be used at the beamlines and experimental stations, respectively. The radiation is polarized with polarization direction in the plane of the electron orbit.

Modern synchrotrons do not use bending magnets anymore, but undulators. An undulator is an arrangement of dipole magnets. In fig. 3.4 the scheme of an undulator is shown. In its alternating static field the electrons oscillate perpendicular to their path. The oscillation direction depends on the arrangement of the magnets and thus it is possible to vary between horizontally and vertically linear polarized light on the one hand and circular polarized light on the other hand. The former effect allows polarization dependent measurements without turning the sample.

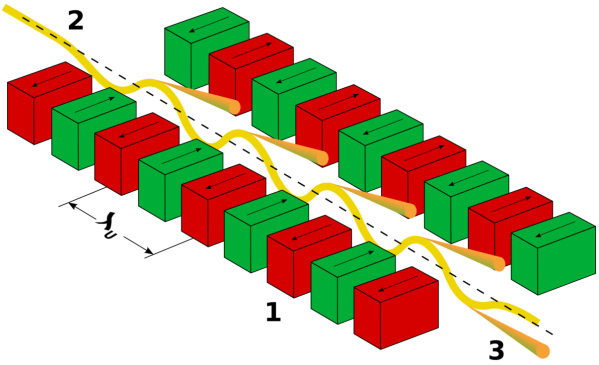

fig. 3.4. An undulator is a special arrangement of magnets (1). It causes an oscillation of the electron beam (2) and emits synchrotron radiation (3). From [16]

Air has a high absorption cross-section in the soft X-ray range, so that the beamline and the experimental station have to be evacuated. The experimental station consists of mainly three chambers: The load lock, where the sample is inserted, a preparation chamber and a main chamber inside a cryostat.
Cleaving under vacuum is important for the measurements, since a clean surface is needed to prevent chemical modifications of the surface which would contribute to the signal.

3.2.2. XAS techniques

X-ray absorption is the quantum mechanical transition due to the interaction of a photon with an electron. There are several methods for measuring such an absorption process in a real experiment:

- Transition mode (TM)
- Fluorescence Yield (FY)
- Total Electron Yield (TEY)

In Transition mode (TM) the intensity of the incoming light (I_0) is compared to the intensity of the transmitted light (I_t). The transmitted intensity is related to the incoming intensity via

$$I_t(\nu) = I_0(\nu)e^{-\mu(\nu)d} \tag{3.11}$$

$\mu(\nu)$ is the energy dependent absorption coefficient and d the thickness of the sample. The TM is no option for soft X-rays because the absorption in the soft X-ray range is so strong that samples would have to be less than 1 μm thick. The Fluorescence Yield (FY) measures the photons which are emitted when the excited electrons decay after the absorption process. FY has a very large probing depth of about 1000 Å and is therefore bulk sensitive, but the FY spectra of heavier elements suffer from strong self absorption so that it is not suitable for cerium samples.
The Total Electron Yield method measures secondary effects which are induced by the absorption of photons. When a core hole decays an *avalanche* of electrons escapes from the sample. The sample is grounded with an amperemeter and a so called *drain current* can be measured which replaces the emitted charges. The drain current is proportional to

the absorption coefficient. For metallic compounds the drain current can be quite large ($\approx 10^{-10}$ A). The method works well and is commonly used although the reason for the proportionality is not fully understood. Here, self absorption can in principle also take place, but is usually negligible because the probing depths are much smaller (about 40 Å for cerium compounds). It is therefore the method of choice for the present investigation.

4. Experiment and analysis

4.1. Experiment on $CeAuAl_3$ and $CeCuAl_3$

The XAS experiments were performed at the DEIMOS beamline at the SOLEIL synchrotron near Paris. XAS spectra at the cerium $M_{4,5}$ edge were measured for linear polarized light with $\mathbf{E} \| c$ and $\mathbf{E} \perp c$. Here, c is the fourfold tetragonal axis. The samples were grown by Christian Franz from the group of Christian Pfleiderer (TU München) [1]. The DEIMOS beamline is an undulator beamline. Thus, the polarization direction can be changed without rotating the sample, which prevents from mistakes. Furthermore, for each polarization the beam hits the same spot of the sample. The photon energy range of DEIMOS is from 350 eV to 2500 eV [17] and thus in the soft X-ray regime. The energy resolution was set to 150 meV.
The samples were inserted into the load lock (see (1) in fig. 4.1). From there they were transferred into the prep chamber (see (2) in fig. 4.1) below the measuring position of the main chamber. The pressure of the prep chamber was $\approx 7 \cdot 10^{-9}$ mbar. The samples were cleaved here and then swiftly transferred into the main chamber (see (3) in fig. 4.1), where the pressure was $\approx 2 \cdot 10^{-10}$ mbar. The samples were post-cleaved and the post was attached to the sample holder with a wire so that it could not fall into the chamber.
The spectra were calculated using the program XTLS8.30 by Arata Tanaka.

4.2. Low temperature

4.2.1. Data

The measured polarization dependent spectra at T = 2 K are shown in fig. 4.2. Both samples exhibit a strong polarization dependence. The polarization dependence of $CeAuAl_3$ is stronger than that of $CeCuAl_3$. A closer look at the M_5 edges with polarization direction $\mathbf{E} \perp c$ shows that the ratio of the shoulders is different for both compounds.

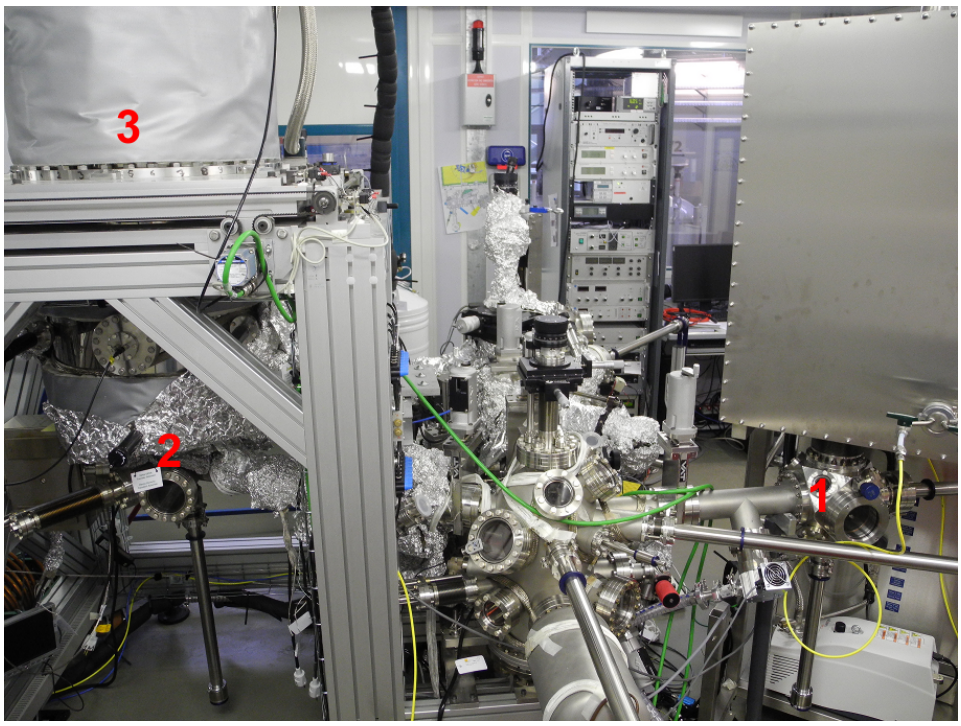

fig. 4.1. Load lock (1), prep chamber (2) and main chamber (3) at the DEIMOS beamline.

While for $CeAuAl_3$ the left shoulder is higher than the right one, it is the other way around for $CeCuAl_3$. Both aspects are indications that both compounds might have different ground state symmetries.

4.2.2. Analysis

$CeAuAl_3$

First, the data at 2 K, which is above the ordering temperature of $T_N = 1.32$ K, were analyzed in order to determine the ground state wave function. The reduction factors for the Hartree-Fock values were fitted to the isotropic spectrum $(I_\parallel + 2I_\perp)/3$ as described in section 3.1.4. The resulting reduction factors are $r_{C,4f} = 0.577$ and $r_{C,3d4f} = 0.780$ for the Coulomb and $r_{\zeta,4f} = 1.0023$ and $r_{\zeta,3d} = 0.956$ for the spin orbit interactions. The isotropic spectrum (dashed lines) and its best fit (solid lines) are shown at the bottom of fig. 4.3.
At 2 K only the CEF ground state is populated because, according to neutron scattering, the first excited CEF state is at 5.1 meV which corresponds to about 60 K [18]. Possible wave functions are a $\Gamma_6 = \left|\pm\frac{1}{2}\right\rangle$ or a $\Gamma_7^1 = \alpha\left|\pm\frac{5}{2}\right\rangle \pm \sqrt{1-\alpha^2}\left|\mp\frac{3}{2}\right\rangle$ (see section 2.2). As a starting point, the data at 2 K are compared to the calculated spectra of the

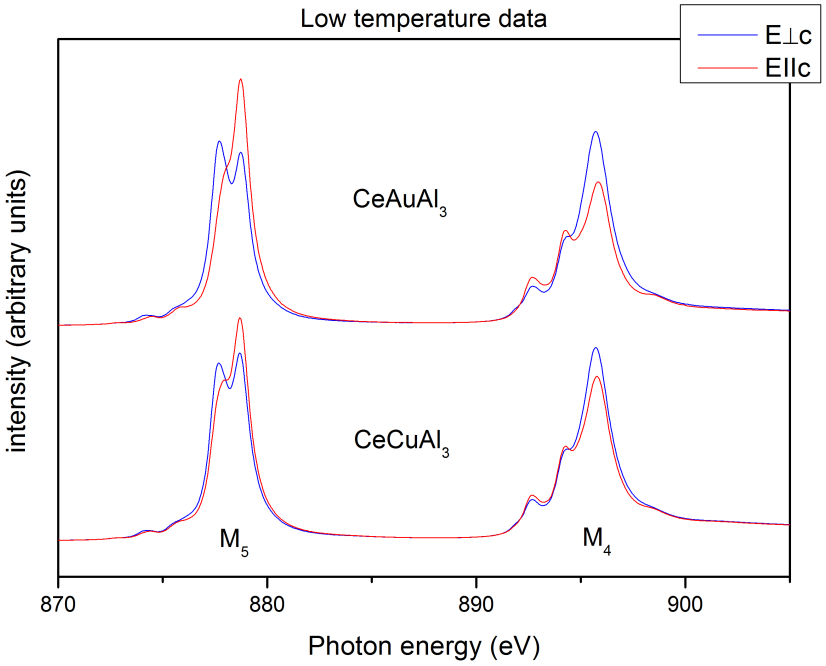

fig. 4.2. Experimental spectra of $CeAuAl_3$ and $CeCuAl_3$ with polarization direction parallel (red) and perpendicular (blue) to the c-axis.

pure $\left|J_z = \pm\frac{1}{2}\right\rangle$ (Γ_6), a pure $\left|J_z = \mp\frac{3}{2}\right\rangle$ corresponding to a Γ_7^1 with $\alpha = 0$, and a pure $\left|J_z = \pm\frac{5}{2}\right\rangle$ corresponding to a Γ_7^1 with $\alpha = 1$. The results of this comparisons are shown in fig. 4.3. The Γ_6 ($\left|J_z = \pm\frac{1}{2}\right\rangle$) describes the data best although not perfectly. The pure $\left|J_z = \mp\frac{3}{2}\right\rangle$ ($\alpha = 0$) fits worse and when considering that a pure $\left|J_z = \mp\frac{3}{2}\right\rangle$ is most unlikely in the present tetragonal point symmetry, a Γ_7^1 ground state can even be excluded because an admixture of $\left|J_z = \pm\frac{5}{2}\right\rangle$ would make the fit worse (see fit for Γ_7^1 with $\alpha = 1$). In total, by exclusion, it is concluded that the Γ_6 must be the CEF ground state of $CeAuAl_3$ and these findings are in agreement with inelastic neutron scattering data by D.T. Adroja [18]. However, how can the fit be improved?
In order to account for possible depolarizations, it was tried to simulate the data with a Γ_6 ground state plus a certain amount of isotropic spectra as follows:

$$\begin{aligned} I_{\parallel c,exp} &= (1-\xi) I_{\parallel c,calc} + \xi I_{iso} \\ I_{\perp c,exp} &= (1-\xi) I_{\perp c,calc} + \xi I_{iso} \end{aligned} \tag{4.1}$$

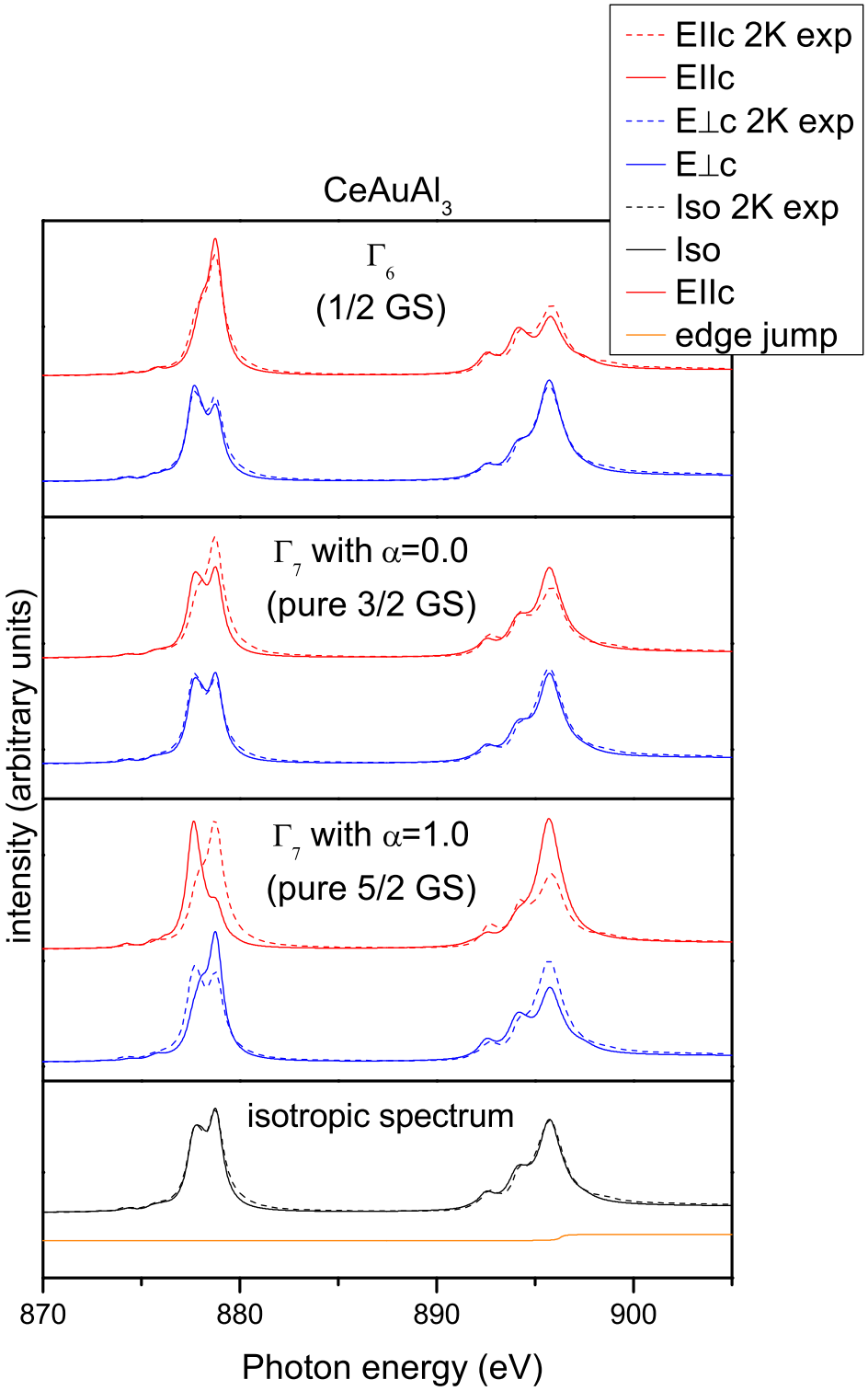

fig. 4.3. Plots of the three pure J_z states as well as the isotropic spectrum and the edge jump are shown (from top to bottom). Dashed lines represent the measurement, solid lines the calculation.

where $I_{\parallel c,exp}$ and $I_{\perp c,exp}$ are the measured intensities parallel and perpendicular to the c-axis, $I_{\parallel c,calc}$ and $I_{\perp c,calc}$ are the calculated ones and I_{iso} is the isotropic intensity. ξ denotes the proportion of the isotropic spectrum.

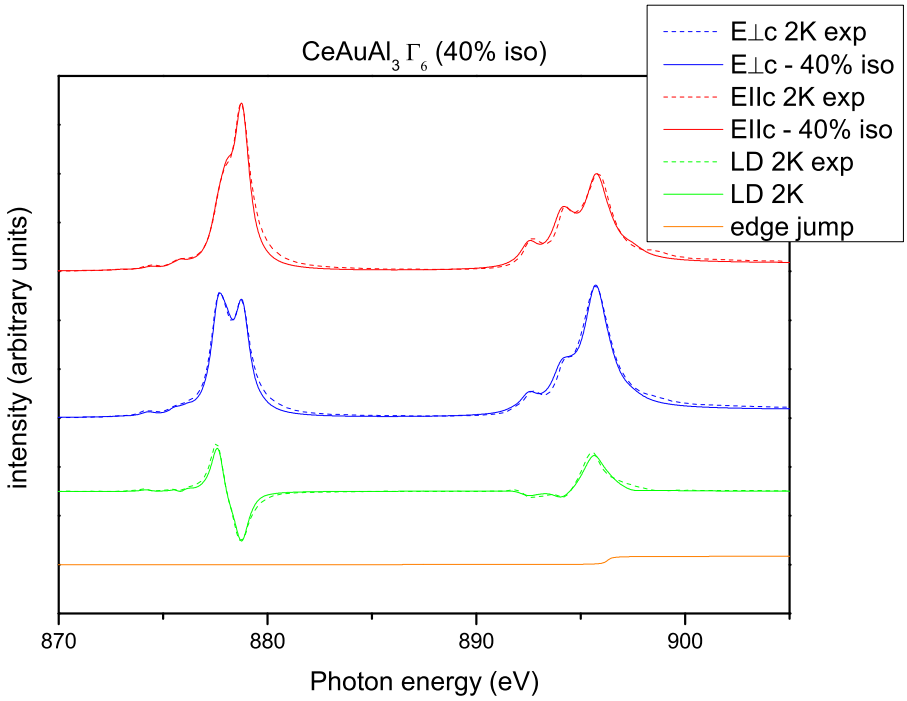

fig. 4.4. Low T fit assuming a Γ_6 ground state. The intensities were calculated mixing 40% ($\xi = 0.40$) of the isotropic spectrum into the polarization dependent spectra. Dashed lines represent the measurement, solid lines the calculation.

In fig. 4.4 the resulting fit to the respective polarizations and also the linear dichroism ($LD = I_\perp - I_\parallel$) are shown. It was found that ξ should be 0.40 with an accuracy of ± 0.05 and so far there is no reasonable explanation for such a large isotropic contribution.
Mixing a Γ_7^1 state with an isotropic spectrum can not give a good result. The pure $\left|J_z = \mp\frac{3}{2}\right\rangle$ and $\left|J_z = \pm\frac{5}{2}\right\rangle$ describe the shoulders of the M_5 edge measured with polarization perpendicular to the c-axis the wrong way around (see fig. 4.3). The same issue applies to the isotropic spectrum compared to the measurement perpendicular to the c-axis. Thus, the isotropic spectrum cannot cancel the mismatch for a Γ_7^1 ground state, it would make it worse instead.

$CeCuAl_3$

The 2 K data were analyzed in order to determine the ground state wave function. 2 K was chosen, although this is below the ordering temperature ($T_N = 2.8$ K), because the lowest excited state is expected at 1.3 meV which corresponds to about 15 K [6] so that at 2 K only the ground state is populated [1]. By fitting the isotropic spectrum, the reduction factors for the Hartree-Fock values were found to be $r_{C,4f} = 0.571$, $r_{C,3d4f} = 0.775$, $r_{\zeta,4f} = 1.0023$ and $r_{\zeta,3d} = 0.959$. The resulting fit (solid lines) as well as the experimental isotropic spectrum (dashed lines) are shown at the bottom of fig. 4.5.
Now the ground state was determined by fitting the polarization dependent spectra at 2 K. The possible ground states are Γ_6 and Γ_7^1 again, since $CeCuAl_3$ has also tetragonal point symmetry. First, a Γ_6 ground state was assumed, but, in contrast to $CeAuAl_3$ the Γ_6 does not describe the data well (see top of fig. 4.5).
Afterwards a Γ_7^1 ground state was studied. If a Γ_7^1 ground state is found, the mixing parameter α is fully determined by fitting the ground state. A pure $\left|J_z = \mp\frac{3}{2}\right\rangle$ state ($\alpha = 0.0$) fits the data well (fig. 4.5), but is forbidden due to the CEF symmetry (see section 2.2). However, it is clear that the ground state has to be a Γ_7^1 with strong emphasis on the $\left|J_z = \mp\frac{3}{2}\right\rangle$ side. A Γ_7^1 state with $\alpha = 0.1$ gives an equally good fit (see fig. 4.5). Therefore the value of α was set to 0.05 ± 0.05. Although the fit is quite good, there are deviations between the experimental and calculated LD (see fig. 4.5). Even a factor cannot fix this. This can happen if there are slight energy shifts between the two polarizations. Unfortunately, the measurement was *not* performed with a reference sample in front of the sample. Values of α higher than 0.1 make the fit worse.
It has to be concluded that the ground state wave function must be

$$|GS\rangle = 0.05 \left|\pm\frac{5}{2}\right\rangle \pm \sqrt{1 - 0.05^2} \left|\mp\frac{3}{2}\right\rangle$$

[1] Magnetic order leads to a Zeeman splitting of the Kramer's doublets. Since the two states of a Kramer's doublet are identical, the magnetic order should have no impact on the CEF wave function.

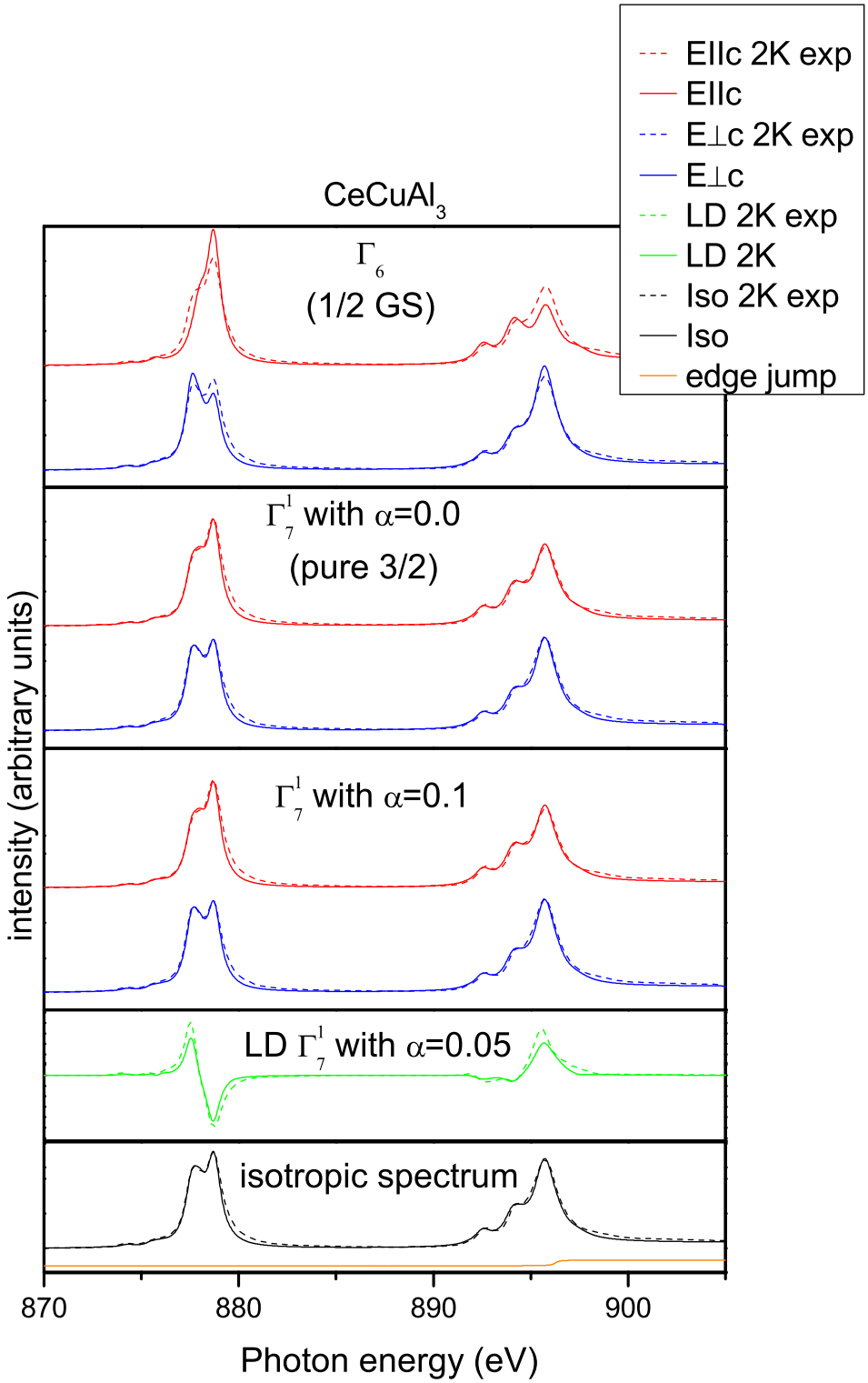

fig. 4.5. Plots of a Γ_6 and a Γ_7^1 state with $\alpha = 0.0$ and $\alpha = 0.1$, the LD of a Γ_7^1 state with $\alpha = 0.05$ (scaled by a factor of 3) as well as the isotropic spectrum and the edge jump are shown (from top to bottom). Both, the Γ_7^1 state with $\alpha = 0.0$ and with $\alpha = 0.1$ fit the experimental data equally good, whereas the Γ_6 does not. There are deviations between the experimental and the measured LD. Dashed lines represent the measurement, solid lines the calculation.

4.3. Temperature dependence

4.3.1. Data

XAS data were also measured as function of temperature in order to follow the population of excited states with increasing temperature (compare 3.1.4). $CeAuAl_3$ was measured at 2, 20, 40, 75, 130, 180 K and $CeCuAl_3$ at 2, 7, 13, 20, 40, 75, 100, 130, 180, 240, and 290 K. The choice of temperatures is based on the CEF excitation energies reported by D.T. Adroja et al. ([18], [6] and see below). Small changes with temperature in the experimental data are better visible in the LD so that the LDs at the two absorption edges are shown for all temperatures, for $CeAuAl_3$ in fig. 4.6 and for $CeCuAl_3$ in fig. 4.7.

The LD of $CeAuAl_3$ decreases with increasing temperature (see fig. 4.6). Qualitatively, it can be stated that this temperature dependence is typical of an order of states with a $|GS\rangle = \Gamma_6$ and a $|1^{st}\rangle = \Gamma_7^1$ with strong emphasis on the $\left|J_z = \mp\frac{3}{2}\right\rangle$ side (and thus a $\left|2^{nd}\right\rangle = \Gamma_7^2$ with strong emphasis on the $\left|J_z = \pm\frac{5}{2}\right\rangle$ side), since the LD of $\left|J_z = \pm\frac{1}{2}\right\rangle$ is largest, the LD of $\left|J_z = \mp\frac{3}{2}\right\rangle$ is smaller and therefore reduces the total LD when it gets populated. The LD of $\left|J_z = \pm\frac{5}{2}\right\rangle$ is the other way around and thus reduces the LD at higher temperatures even further.

For $CeCuAl_3$ the temperature dependence is different (see fig. 4.7). The LD increases from 2 to 40 - 75 K, i.e. the LD at 7 K is already slightly larger than at 2 K. Above 75 K the LD starts to decrease. Following the quantitative considerations of the previous paragraph, this implies a $\left|J_z = \mp\frac{3}{2}\right\rangle$-like ground state as it was found by the analysis of the low temperature data, a Γ_6 first excited state, which increases the LD since it has stronger polarization and a Γ_7^2 second excited state with strong emphasis on the $\left|J_z = \pm\frac{5}{2}\right\rangle$ side. However, since for this compound a fourth level was reported by Adroja et al. [6], a more detailed analysis has to be performed.

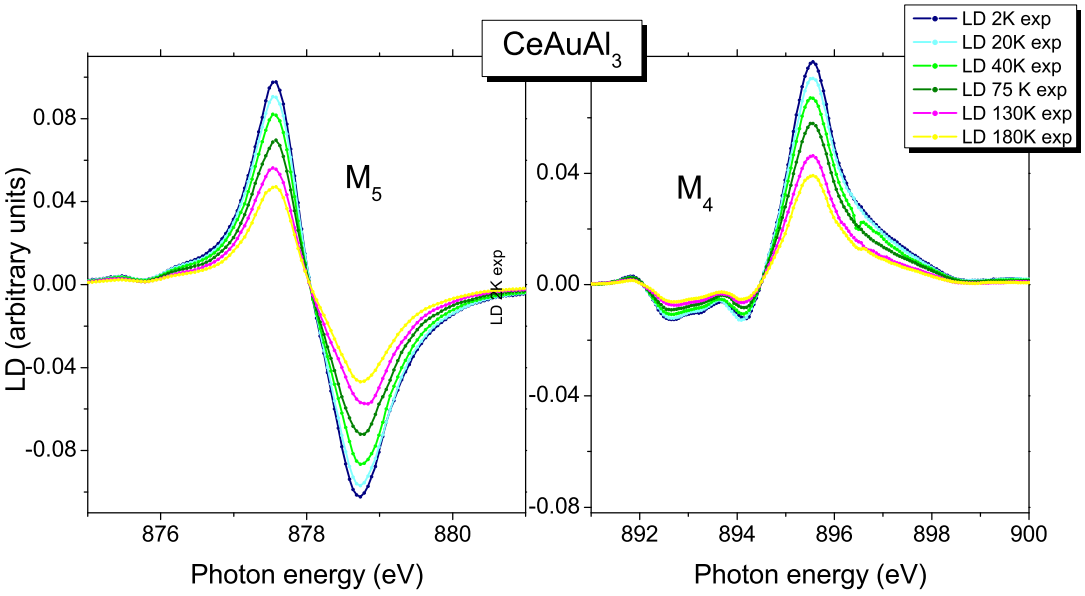

fig. 4.6. Experimental LD of $CeAuAl_3$ for each measured temperature.

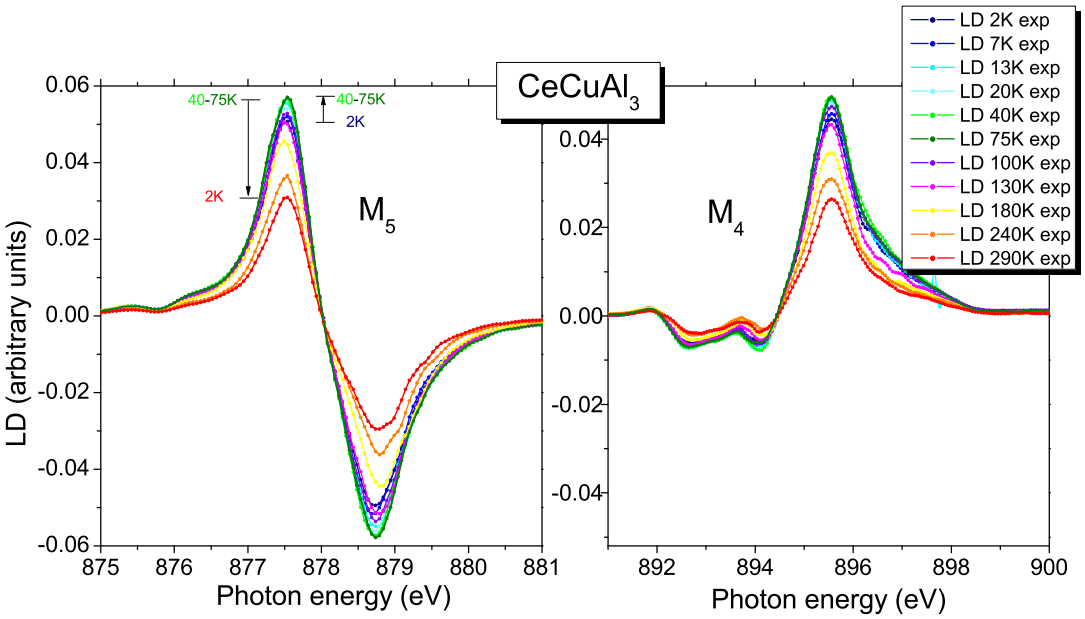

fig. 4.7. Experimental LD of $CeCuAl_3$ for each measured temperature.

4.3.2. Analysis

$CeAuAl_3$

To carry out the analysis of the $CeAuAl_3$ XAS data CEF levels at 0 meV, 5.1 meV and 25.33 meV were used according to D.T. Adroja [18].
The LD is modeled despite the above mentioned problem of a significant amount of isotropic contribution to the data. If present at low temperatures, it must also be present at all other temperatures. The following consideration shows, that an amount ξ of isotropic spectra in the polarized data relates to a reduction in the LD by a factor of $(1-\xi)$ which in the following is used as a scaling factor for the calculated LD.

$$\begin{aligned} LD_{exp} &= I_{\perp c,exp} - I_{\parallel c,exp} \\ &\overset{4.1}{=} ((1-\xi)I_{\perp c,calc} + \xi I_{iso}) - ((1-\xi)I_{\parallel c,calc} + \xi I_{iso}) \\ &= (1-\xi)I_{\perp c,calc} - (1-\xi)I_{\parallel c,calc} \\ &= (1-\xi)(I_{\perp c,calc} - I_{\parallel c,calc}) \\ &= (1-\xi)LD_{calc} \end{aligned} \tag{4.2}$$

Now the net LD at the temperature T, LD(T), is calculated by using the respective occupation numbers N_i for a three level system with ground state ($i=0$) $|GS\rangle$ at 0 meV, first excited state ($i=1$) $|1^{st}\rangle$ at 5.1 meV, and second excited state ($i=2$) $\left|2^{nd}\right\rangle$ at 25.33 meV which are given by a Boltzmann distribution (see 3.9). The occupation numbers for each state and temperature are listed in tab. A.1 in the appendix.
The net LD for a given temperature is then:

$$LD_{exp}(T) = (1-\xi)LD_{calc} \tag{4.3}$$

$$= (1-\xi)(N_0(T)LD_0 + N_1(T)LD_1 + N_2(T)LD_2) \tag{4.4}$$

The LD of the ground state is known, the $N_i(T)$ can be calculated since the energies and temperature are known (see tab. A.1), so that the J_z admixture α of $\left|J_z = \mp\frac{3}{2}\right\rangle$ and $\left|J_z = \pm\frac{5}{2}\right\rangle$ is the only remaining fit parameter since both excited states are of type Γ_7 (see section 4.2.2). The best fit to the data was obtained for $\alpha = 0.2$ with an accuracy of ± 0.1 (see solid lines in fig. 4.8). The good agreement between measured and calculated temperature dependence of the LD is another proof for a Γ_6 ground state. Figure 4.9

shows the resulting CEF scheme of $CeAuAl_3$.

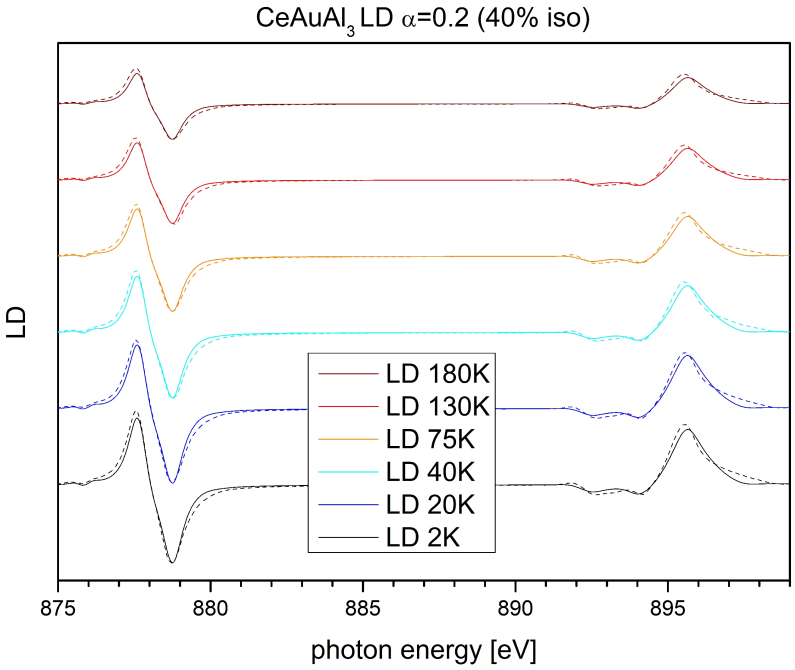

fig. 4.8. LDs of $CeAuAl_3$ for several temperatures with $\alpha = 0.2$. Dashed lines represent the measurement, solid lines the calculation.

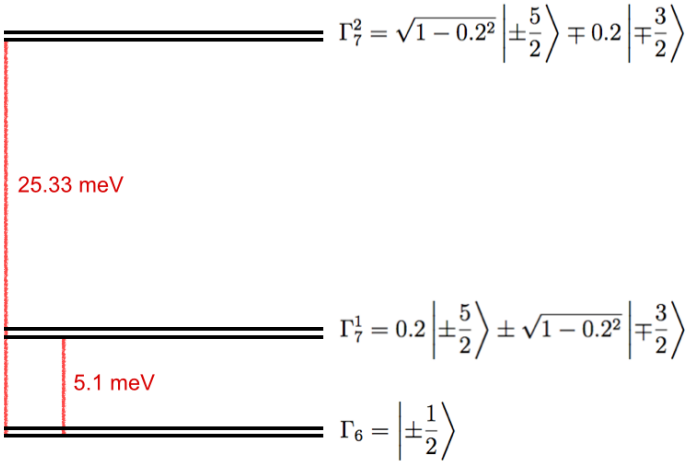

fig. 4.9. Level scheme of $CeAuAl_3$ with the determined CEF states. The mixing parameter α has been determined to be 0.2 ± 0.1.

$CeCuAl_3$

For $CeCuAl_3$ a Γ_7^1 ground state was found by fitting the 2 K spectra so that the mixing parameter α has already been determined. In a normal system, in addition to the ground state at 0 meV, two more CEF levels would be expected. However, Adroja et al. [6] have observed an additional magnetic excitation in their inelastic neutron data (see section 1). The transition energies reported by Adroja et al. are 0, 1.3, 9.8 and 20.5 meV. The temperature dependent data should answer the following questions: 1) Are three or four levels required to describe the temperature dependence of the LD? 2) In the event three levels are sufficient, which of the four energies reported relate to CEF transitions? 3) What is the order of states? In order to answer these questions the LD has been simulated for different models. First, the temperature dependence was simulated with three states in order to find out to what extent the data can be described with an ordinary CEF model (option 1-5, see below), and then in a second step a fourth state was taken into account (option 6-8). The possible combinations of levels are shown in tab. 4.1.

option	**CEF levels**			
	0 meV	1.3 meV	9.8 meV	20.5 meV
1	Γ_7^1	Γ_7^2	Γ_6	-
2	Γ_7^1	-	Γ_7^2	Γ_6
3	Γ_7^1	Γ_6	Γ_7^2	-
4	Γ_7^1	Γ_6	-	Γ_7^2
5	Γ_7^1	-	Γ_6	Γ_7^2
6	Γ_7^1	Γ_7^1	Γ_6	Γ_7^2
7	Γ_7^1	Γ_6	Γ_6	Γ_7^2
8	Γ_7^1	iso	Γ_6	Γ_7^2

tab. 4.1. The temperature dependence of the experimental LD is compared to the calculated LDs of these 8 options.

Option 1 & 2 The LD resulting from option 2 is shown in fig. 4.10. It is maximum at 2 to 20 K. The LD almost remains of the same size (≈ 0.4 arbitrary units (a.u.), left side of M_5 edge) for these temperatures and is smaller than the maximum of the experimental LD (≈ 0.55 a.u., left side of M_5 edge). The calculated LD of option 2 starts decreasing above 20 K and even changes its directions for temperatures higher than 75 K due to the occupation of the $\left|J_z = \pm\frac{5}{2}\right\rangle$-like Γ_7^2 state. This is in total disagreement with the experimental LD. Thus, option 2 can be excluded.
Option 1 can be excluded as well, since the Γ_7^2 state is here at a lower energy, causing the LD to decrease more rapidly at low temperatures.

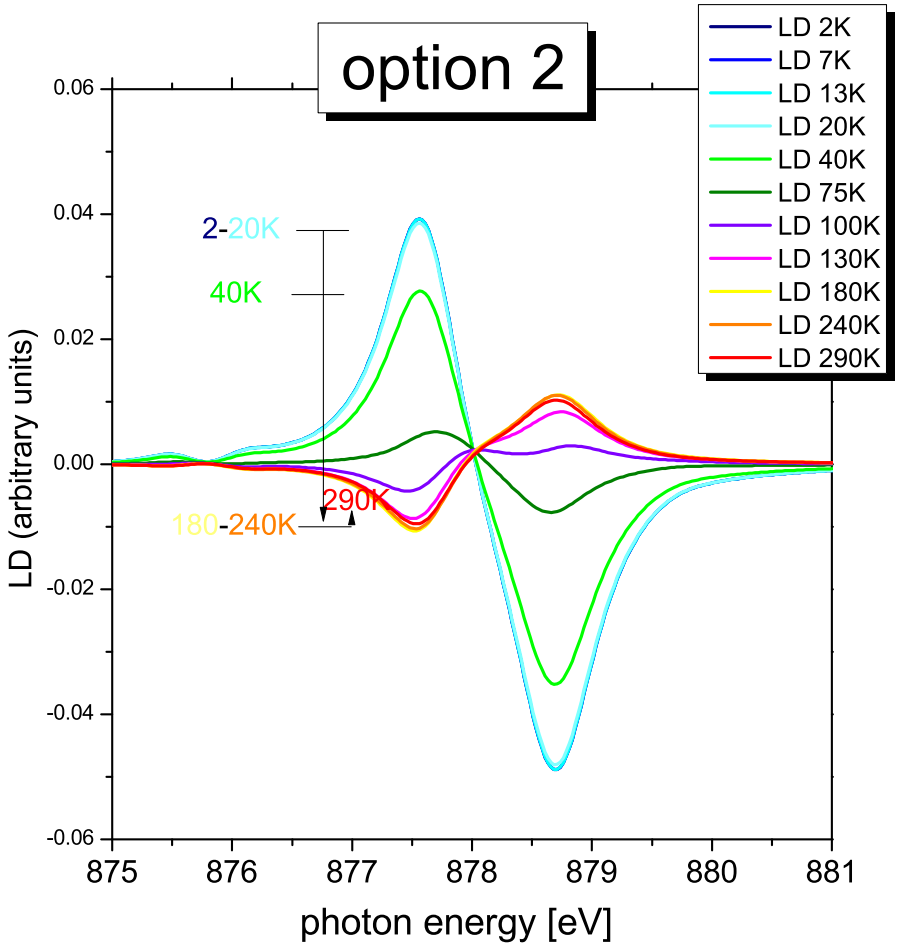

fig. 4.10. LD of the M_5 edge of option 2
(Γ_7^1 ground state, - at 1.3 meV, Γ_7^2 at 9.8 meV, Γ_6 at 20.5 meV)

Option 3 The simulated LD of option 3 (see fig. 4.11) increases from 2 K to 20 K. The LDs at 20 and 40 K are of the same size of ≈ 0.7 a.u. (left side of M_5 edge) and thus too large to describe the temperature dependence of the experimental LD correctly. Above 40 K, the simulated LD decreases, whereas the experimental LD has its maximum at 40 to 75 K. Thus option 3 does not describe the temperature dependence correctly and can be excluded.

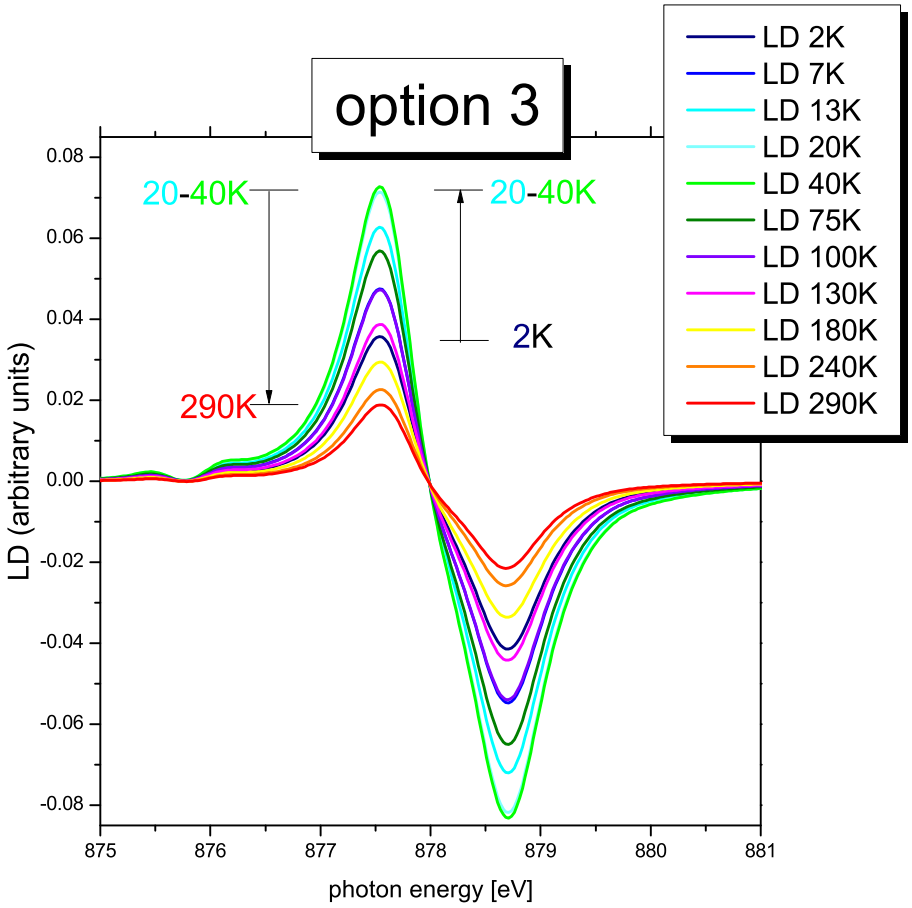

fig. 4.11. LD of the M_5 edge of option 3
(Γ_7^1 ground state, Γ_6 at 1.3 meV, Γ_7^2 at 9.8 meV, - at 20.5 meV)

Option 4 (see fig. 4.12) has a minimum LD at 2 K. It strongly increases up to its maximum at 40 to 75 K ($\approx$ 0.8 a.u., left side of M_5 edge). Although the maximum LD at 40 to 75 K corresponds to the data, option 4 can be excluded, since for these and also for all higher measured temperatures the LD is too large to describe the experimental data correctly.

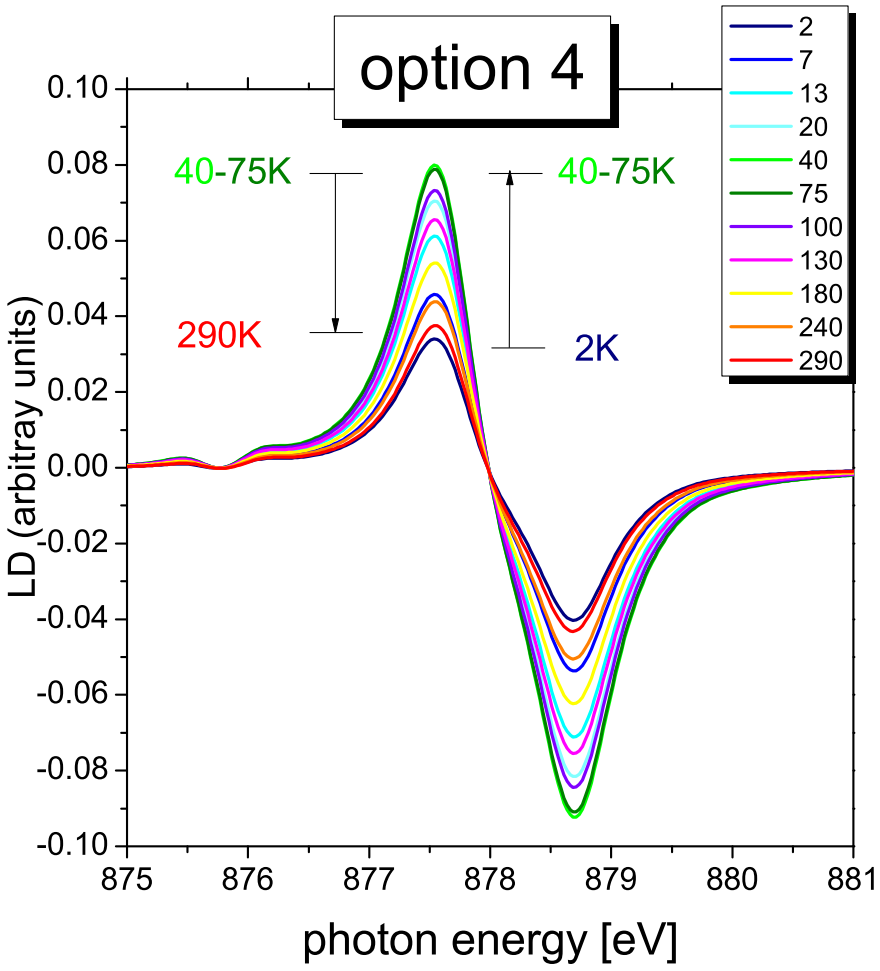

fig. 4.12. LD of the M_5 edge of option 4
(Γ_7^1 ground state, Γ_6 at 1.3 meV, - at 9.8 meV, Γ_7^2 at 20.5 meV)

Option 5 gives the best fit for the temperature dependent $CeCuAl_3$ data with 3 states (see fig. 4.13). It has its maximum LD at 75 K which corresponds to the experimental result. The total size of the LD calculated for this option is also in the range of the size of the experimental LD ($\approx$ 0.5 a.u., left side of M_5 edge). However, there remains the issue that the (small) temperature dependence of the experimental LD (increasing) between 2 and 20 K is not reproduced by option 5.

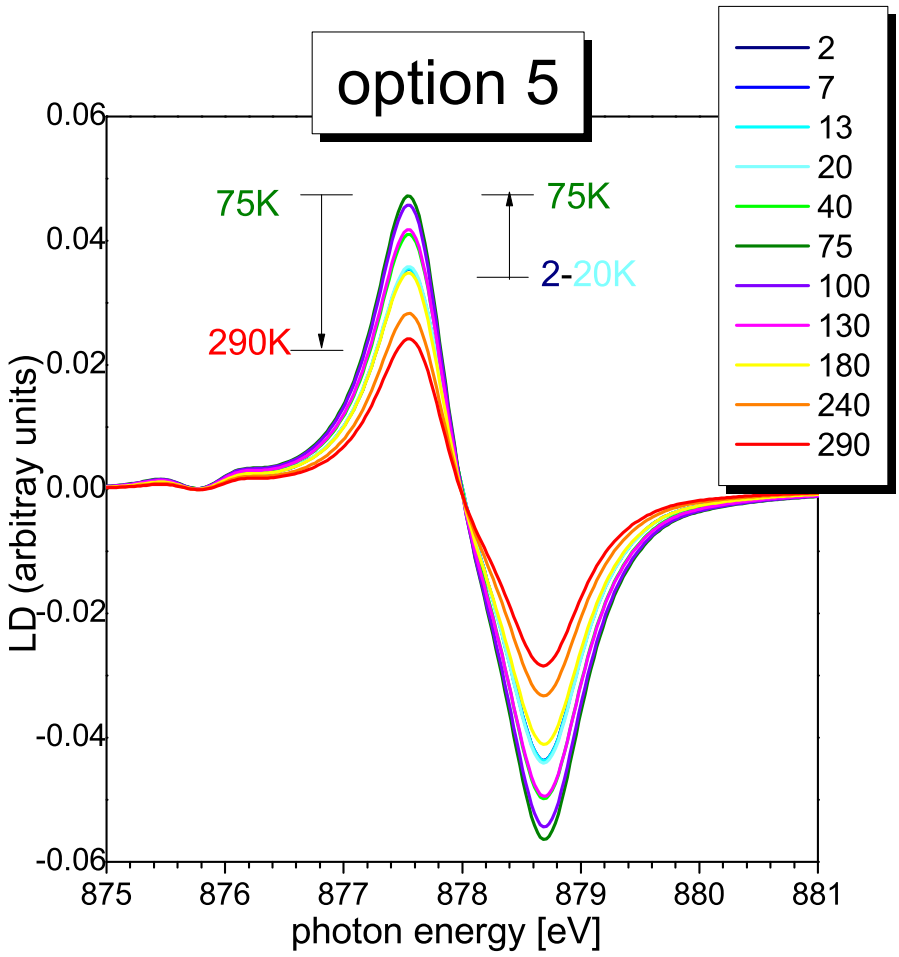

fig. 4.13. LD of the M_5 edge of option 5
(Γ_7^1 ground state, - at 1.3 meV, Γ_6 at 9.8 meV, Γ_7^2 at 20.5 meV)

Option 6 gives a fit which is almost identical to the one of option 5, it only reduces the change of the LD with temperature (see fig. 4.14). This is not surprising since the ground state and the state at 1.3 meV have the same symmetry, thus putting more emphasis on the Γ_7^1, i.e. almost $\left|J_z = \mp\frac{3}{2}\right\rangle$-like symmetry (see occupation numbers, tab. A.4 in the appendix). This option also fails to reproduce the temperature dependence between 2 and 20 K.

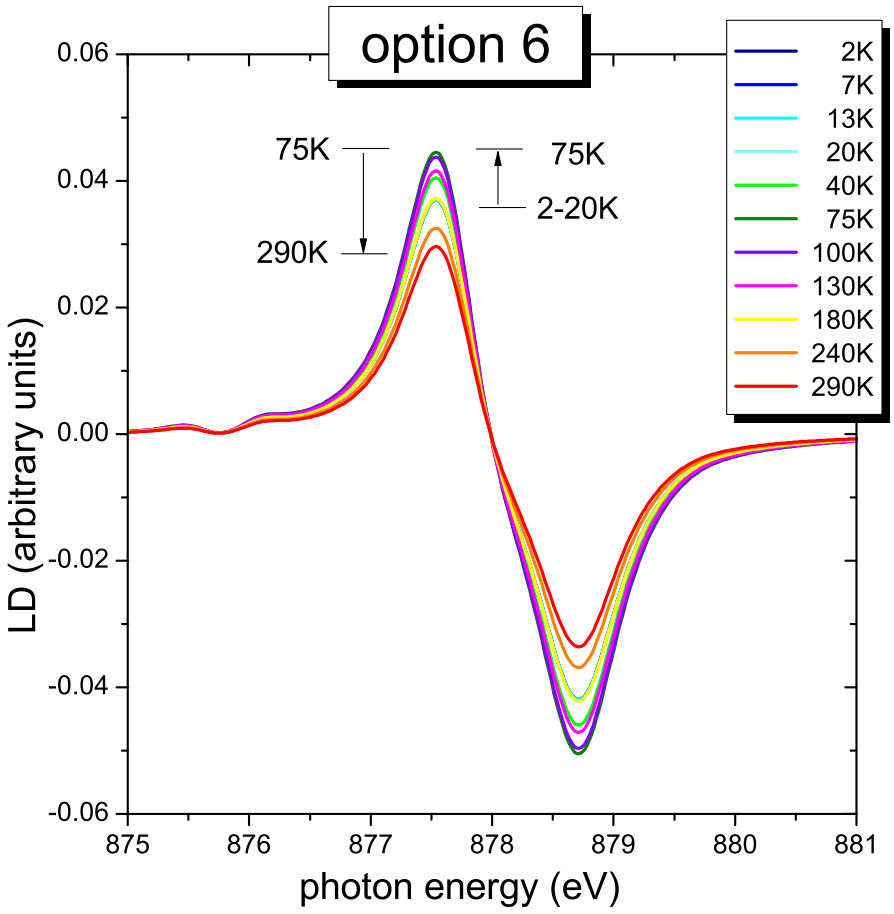

fig. 4.14. LD of the M_5 edge of option 6
(Γ_7^1 ground state, Γ_7^1 at 1.3 meV, Γ_6 at 9.8 meV, Γ_7^2 at 20.5 meV)

Option 7 leads to the same issue as options 3 and 4. Due to the occupation of the low lying $\left|J_z = \pm\frac{1}{2}\right\rangle$ state, the LD already becomes too large at 13 K (see fig. 4.15). It remains too large over a large temperature interval because there is more weight on the $\left|J_z = \pm\frac{1}{2}\right\rangle$ symmetry. Option 7 can thus be excluded.

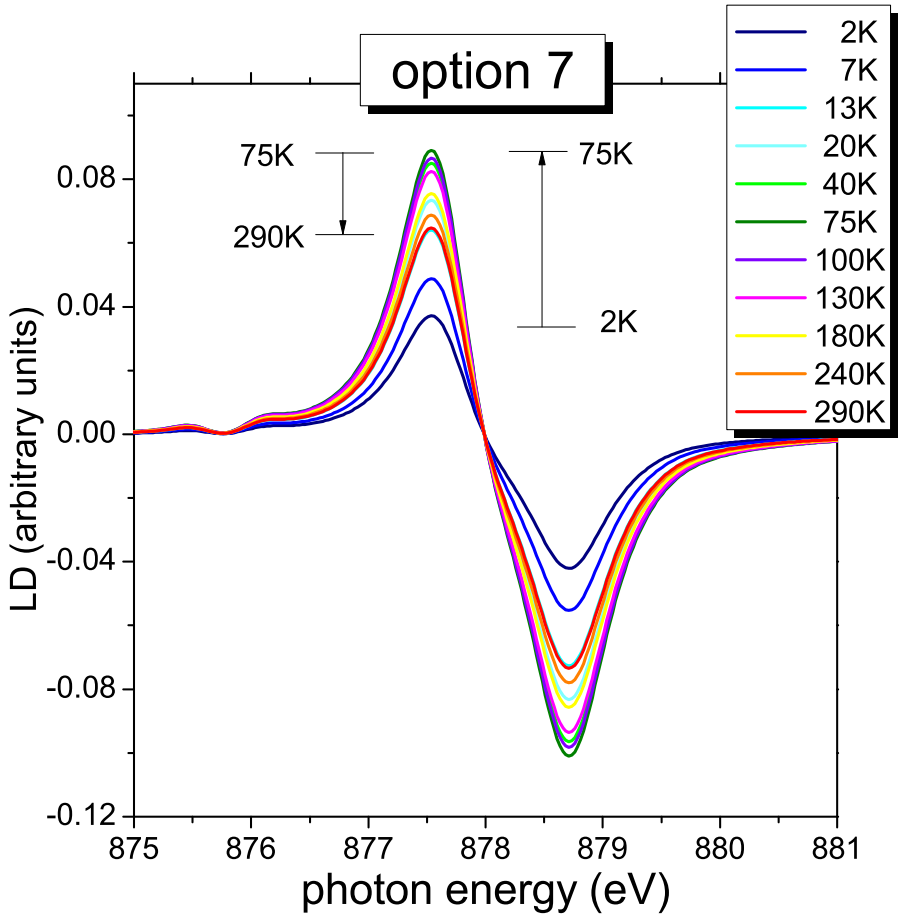

fig. 4.15. LD of the M_5 edge of option 7
(Γ_7^1 ground state, Γ_6 at 1.3 meV, Γ_6 at 9.8 meV, Γ_7^2 at 20.5 meV)

Option 8 (see fig. 4.16) can also be excluded since the LD of the isotropic state at 1.3 meV is zero, i.e. reduces the total LD with increasing population. The LD mainly decreases from 2 to 290 K but increases in between from 20 to 75 K.

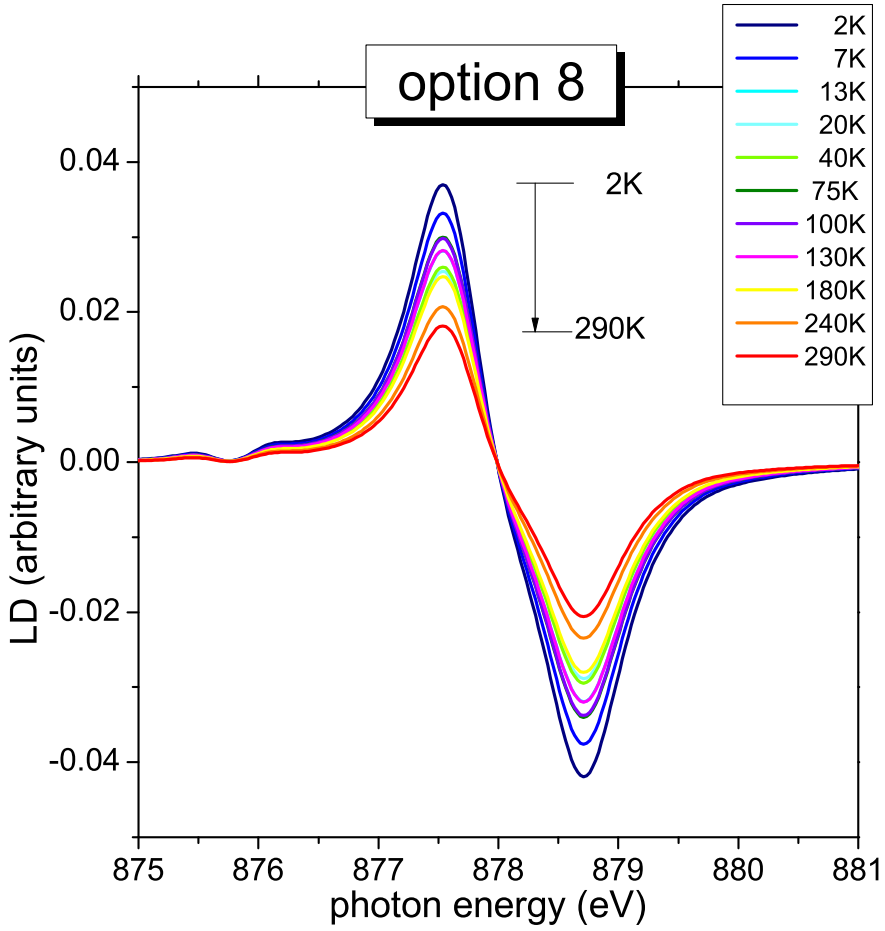

fig. 4.16. LD of the M_5 edge of option 8
(Γ_7^1 ground state, $|iso\rangle$ at 1.3 meV, Γ_6 at 9.8 meV, Γ_7^2 at 20.5 meV)

5. Conclusion & Outlook

Linear polarized X-ray absorption data at the cerium M-edges have been measured and were analyzed with a full multiplet routine in order to determine the crystal-electric field schemes of $CeAuAl_3$ and $CeCuAl_3$. For $CeCuAl_3$ an extra excitation due to crystal-field-phonon coupling had been reported by Adroja et al. and the scope of this thesis was to confirm these findings and to determine the CEF wave functions' symmetry.

For $CeAuAl_3$, a Γ_6 ground state yields the best, although not perfect, fit to the data. Mixing a substantial amount of isotropic spectrum improves the agreement between data and simulations. Further investigations will be needed to understand the origin of the large isotropic amount. The LD decreases continuously with increasing temperature and the temperature dependence can be described with a Γ_7^1 state at 5.1 meV and a Γ_7^2 at 25.33 meV, thus confirming the transition energies found by neutron scattering [18].

For $CeCuAl_3$ a strongly $\left|J_z = \mp\frac{3}{2}\right\rangle$ like Γ_7^1 ground state with $\alpha = 0.05\pm0.05$ was found. The fit to the spectra seems to be quite good although the LD shows some deviations between the calculated and the measured spectra.
The LD at first increases with rising temperature and then decreases continuously for T > 75 K. The temperature dependence was analyzed by discussing several options of levels and orders of states. The best agreement was given by option 5 (Γ_7^1 at 0 meV, Γ_6 at 9.8 meV and Γ_7^2 at 20.5 meV) but it does not describe the changes with temperature between 2 and 20 K. Thus there has to be something that causes an increase of LD at these low temperatures.
A low lying fourth state at 1.3 meV could lead to this increase. Since the ground state is already an almost pure $\left|J_z = \mp\frac{3}{2}\right\rangle$ (Γ_7^1 with $\alpha = 0.05$), the only by symmetry allowed state that would increase the LD is the Γ_6. It has been shown that this state can not be at 1.3 meV (see option 7). Thus, the LD of the state at 1.3 meV has to be between the LD of $\left|J_z = \mp\frac{3}{2}\right\rangle$ and the LD of $\left|J_z = \pm\frac{1}{2}\right\rangle$, since the increase of the LD between 2 K

and 13 K can not be described by the occupation of the $\left|J_z = \pm\frac{1}{2}\right\rangle$ state at 9.8 meV (see occupation numbers, tab. A.3). Therefore, the state at 1.3 meV has to be of a symmetry which is not defined within the normal CEF picture. This is in contrast to the interpretation of the neutron data. Adroja et al. fitted the excitations at 1.3 and 20.5 meV within a CEF model and suggested the intensity at 9.8 meV must be of different origin.

To give evidence to the existence of a low lying fourth state in $CeCuAl_3$, further investigations will be needed. Raman measurements might be a good option to obtain further insight.

A. Occupation numbers

T(K)	N_0	N_1	N_2
2	1.000	0.000	0.000
20	0.951	0.049	0.000
40	0.814	0.185	0.001
75	0.678	0.308	0.013
130	0.575	0.365	0.060
180	0.522	0.376	0.102

tab. A.1. Occupation numbers $N_i(T)$ of a three level system with states at 0 (N_0), 5.1 (N_1)and 25.33 meV (N_2) for the respective temperatures.

T(K)	N_0	N_1	N_2
	1 / 2 / 3	1 / 2 / 3	1 / 2 / 3
2	0.999 / 0.999 / 1.000	0.001 / 0.001 / 0.000	0.000 / 0.000 / 0.000
7	0.896 / 0.896 / 1.000	0.104 / 0.104 / 0.000	0.000 / 0.000 / 0.000
13	0.761 / 0.761 / 1.000	0.239 / 0.239 / 0.000	0.000 / 0.000 / 0.000
20	0.679 / 0.680 / 0.997	0.319 / 0.320 / 0.003	0.002 / 0.000 / 0.000
40	0.573 / 0.592 / 0.943	0.393 / 0.406 / 0.055	0.033 / 0.002 / 0.002
75	0.491 / 0.538 / 0.793	0.401 / 0.440 / 0.174	0.108 / 0.023 / 0.033
100	0.459 / 0.512 / 0.708	0.394 / 0.440 / 0.227	0.147 / 0.047 / 0.066
130	0.433 / 0.488 / 0.634	0.386 / 0.434 / 0.264	0.181 / 0.078 / 0.102
180	0.408 / 0.457 / 0.556	0.375 / 0.421 / 0.296	0.217 / 0.122 / 0.148
240	0.390 / 0.433 / 0.502	0.367 / 0.406 / 0.312	0.243 / 0.161 / 0.186
290	0.381 / 0.418 / 0.473	0.362 / 0.397 / 0.319	0.257 / 0.184 / 0.208

tab. A.2. Occupation numbers of each state, temperature and possible combination of states for the three states systems. The different combinations of states are marked with different colors. Red: levels at 0, 1.3 and 9.8 meV; green: 0, 1.3 and 20.5 meV; blue: 0, 9.8, 20.5 meV

T(K)	N_0	N_1	N_2	N_3
2	0.999	0.001	0.000	0.000
7	0.896	0.104	0.000	0.000
13	0.761	0.239	0.000	0.000
20	0.679	0.319	0.002	0.000
40	0.573	0.393	0.033	0.001
75	0.481	0.393	0.106	0.020
100	0.440	0.378	0.141	0.041
130	0.405	0.361	0.169	0.065
180	0.368	0.338	0.196	0.098
240	0.341	0.320	0.212	0.127
290	0.326	0.310	0.220	0.144

tab. A.3. Occupation numbers of a 4 states system with levels at 0, 1.3, 9.8 and 20.5meV.

T(K)	$N(\Gamma_7^1)$		$\frac{N(\Gamma_7^2)}{N(\Gamma_6)}$	
	option 5	option 6	option 5	option 6
2	1.000	1.000	0.000	0.000
7	1.000	1.000	0.000	0.000
13	1.000	1.000	0.000	0.000
20	0.997	0.998	0.000	0.002
40	0.943	0.965	0.036	0.045
75	0.793	0.874	0.190	0.191
100	0.708	0.818	0.291	0.289
130	0.634	0.766	0.386	0.385
180	0.556	0.706	0.500	0.502
240	0.502	0.661	0.596	0.596
290	0.473	0.636	0.652	0.652

tab. A.4. Comparison of occupation numbers for option 6 and option 5. The first and the second column show the total occupation of the Γ_7^1 state, columns 3 and 4 show the ratio of the occupation number of the state at 20.5 meV to the occupation number of the state at 9.8 meV. It can be seen, that the additional Γ_7^1 state at 1.3 meV acts as a buffer for the ground state.

Bibliography

[1] C. Franz. *Untersuchung von Quantenphasenübergängen bei fehlender Inversionssymmetrie*. PhD thesis, Technische Universität München, 2014.

[2] M. Klicpera and P. Javorsky. Study of electronic properties in $RCu_{1-x}Au_xAl_3$ compounds, where R=Ce, La. *Journal of Magnetism and Magnetic Materials*, 2014.

[3] E. Bauer et al. Heavy Fermion Superconductivity and Magnetic Order in Noncentrosymmetric $CePt_3Si$. *Phys. Rev. Lett.*, 92(027003), 2004.

[4] S. Paschen, E. Felder, and H.R. Ott. Transport and thermodynamic properties of $CeAuAl_3$. *The European Physical Journal B*, 2, 1998.

[5] E. Bauer, N. Pillmayr, E. Gratz, G. Hilscher, D. Gignoux, and D. Schmitt. On the Behaviour of the New Kondo Lattice $CeCuAl_3$. *Zeitschrift für Physik B Condensed Matter*, 67, 1987.

[6] D. T. Adroja, A. del Moral, C. de la Fuente, A. Fraile, E. A. Goremychkin, J. W. Taylor, A. D. Hillier, and F. Fernandez-Alonso. Vibron Quasibound State in the Noncentrosymmetric Tetragonal Heavy-Fermion Compound $CeCuAl_3$. *PRL*, 2012.

[7] P. Thalmeier and P. Fulde. Bound State between a Crystal-Field Excitation and a Phonon in $CeAl_2$. *PRL*, 1982.

[8] H. Bethe. Termaufspaltung in Kristallen. *Annalen der Physik*, 395(133), 1929.

[9] J. H. van Vleck. Quantum mechanics - the key to understanding magnetism. *Science*, 201(4351), 1978.

[10] J. Jensen and A.R. Mackintosh. *Rare Earth Magnetism: Structures and Excitations*. Clarendon Press, 1991.

[11] P. Hansmann. Crystal-field ground states of rare earth materials determined by linear dichroism: A feasibility study and its experimental proof. Master's thesis, University of Cologne, 2007.

[12] T. Willers. *Spectroscopic Investigations of the Crystal Field and Kondo Effect in 4f Heavy-Fermion Systems*. PhD thesis, University of Cologne, 2011.

[13] T. Willers. Is XAS a bulk sensitive technique to determine crystal-field ground states in Ce intermetallics? Master's thesis, University of Cologne, 2007.

[14] R.D. Cowan. *The Theory of Atomic Structure and Spectra*. University of California Press, 1981.

[15] P. Körner. Cubic and giant hexagonal crystal fields in rare earth intermetallic compounds. Master's thesis, University of Cologne, 2008.

[16] www.en.wikipedia.org.

[17] www.synchrotron-soleil.fr.

[18] D. T. Adroja. private communication, november 2014. Neutron experiments on $CeAuAl_3$.

Acknowledgement

I would like to thank Prof. Paul H. M. van Loosdrecht for the chance to work on this topic, and Prof. Mohsen Abd-Elmeguid for doing the second supervision.

Furthermore I would like to thank Andrea Severing for her excellent support.

Many thanks to the people in the office: Fabio Strigari and Martin Sundermann for the discussions that brought me closer to the topic.
Thanks to Jonas Weinen for his LaTeX support and - of course - coffee and thanks to Siegurt Skoda for many funny conversations.

I would like to thank Raphael German for his dedication with respect to the Raman measurements.

And finally thanks to the whole van Loosdrecht group for the amicable atmosphere.

Erklärung

Hiermit erkläre ich, dass ich die vorliegende Arbeit selbstständig verfasst, alle verwendeten Quellen und Hilfsmittel im Quellenverzeichnis genannt, sowie Zitate als solche gekennzeichnet habe.

Köln, den 19. Januar 2015

Paul Rosenberger